Uronium from X-ray Desorbed Solid Urea Enables Attomole Sensitivity to Amines and Semivolatiles

Aleksei Shcherbinin,[*,†,‖] Henning Finkenzeller,[*,‡,†,‖] Fariba Partovi,[†] Netta Vinkvist,[§] Jussi Kontro,[†] Matthew Boyer,[‡] Joona Mikkilä,[†] Siddharth Iyer,[¶] Jyri Mikkilä,[†] Paxton Juuti,[†] Nina Sarnela,[‡] Juha Kangasluoma,[‡] and Matti Rissanen[¶,§]

†*Karsa Ltd., Helsinki, Finland*
‡*Institute for Atmospheric and Earth System Research / Department of Physics, Faculty of Science, University of Helsinki, Helsinki, Finland*
¶*Aerosol Physics Laboratory, Physics Unit, Faculty of Engineering and Natural Sciences, Tampere University, Tampere, Finland*
§*Department of Chemistry, Faculty of Science, University of Helsinki, Helsinki, Finland*
‖*author with equal contributions*

E-mail: Aleksei.Shcherbinin@Karsa.fi; Henning.Finkenzeller@Helsinki.fi

Abstract

The vast chemical diversity of compounds relevant for gas-phase molecular analytics necessitates the combination of complimentary ionization approaches optimized for specific classes to enable comprehensive mass spectrometric detection. For the ionization of weakly polar volatile organic compounds (VOCs), chemical ionization at low pressure (e.g. proton- or charge-transfer) is more suitable. Negative mode ionization at ambient pressure has delivered superior performance for moderately and highly polar acidic compounds. Numerous alternative positive mode ionization techniques have been explored to detect basic and polar neutral compounds, for which negative polarity and low-pressure ionization techniques have shown insufficient performance. Several ion attachment reagents, such as ammonia and amines, have been previously proposed for more sensitive and soft ionization at ambient and reduced pressures. However, these reagents are often reactive, toxic, and difficult to control, impeding their applicability and operability. Inspired by these challenges, we explored uronium as a sensitive and robust reagent cation for ionizing moderately polar, basic, and neutral compounds at ambient pressure. Urea, a solid chemical safe to humans with negligible vapor pressure under normal circumstances, is desorbed by x-ray irradiation, forming the uronium ion. We experimentally determined the calibration factors and behavior under different humidities for several semivolatile organic compounds (SVOCs), amines, and ammonia, and explored the ionization characteristics using theory. In laboratory measurements of α-pinene and dimethyl sulfide (DMS) oxidation systems we characterized how uronium chemical ionization complements other ionization. Beyond excellent sensitivities to several key components (including amines, dimethyl sulfoxide (DMSO), pyridine, N-Methyl-2-pyrrolidone (NMP), verbenone and dimethylformamide (DMF)) allowing detection at the low to mid parts per quadrillion per volume (ppqv) level - achieved due to uronium's tendency to selectively form strong ion-molecular clusters – and low susceptibility of these cluster formation properties to sample hu-

midity changes, the marked benefit of uronium CIMS lies in the trivial handling of the reagent supply and long-term stability of the ion production system. Overall, uronium CIMS represents an innovative technique with significant potential for standardization and wide applicability, given its demonstrated detection efficiency that complements negative mode and low-pressure ionization techniques, safety, and low maintenance requirements.

Introduction

Chemical Ionization Mass Spectrometry (CIMS) is an essential analytical technique for the direct gas-phase analysis of a wide range of compounds in multiple applications including industrial process control,[1] air quality monitoring,[2] food science,[3] medical research,[4] and atmospheric science.[5] Multiple customized approaches have been developed in pursuit of the efficient detection of the vast spectrum of molecules that exist in the gas phase. The polarity,[6] pressure,[7] temperature,[8,9] and electronic structural features[10] of the reagent ions define the dimensionality of the chemical ionization (CI) regimes, resulting in a specific selectivity and sensitivity profile of a given ionization scheme for particular compounds.

Proton-transfer-reaction mass spectrometry (PTR-MS) using hydronium as a reagent ion at low pressure has become a widely adopted technique for analysing VOCs.[11] While it is an excellent analysis tool for less polar and more volatile molecules, it is, by nature, less selective and more fragmenting towards more functionalized species.[12–14] Polar acidic and highly oxygenated species are best detected by negative-mode chemical ionization, such as nitrate, bromide, and iodide CIMS.[15–18] A number of techniques have been proposed for the sensitive detection of several SVOCs, often constituting lowly oxygenated, moderately polar, and basic molecules – compound classes for which PTR-MS and negative mode ion attachment techniques exhibit reduced sensitivity. The most notable methods are ammonium[19] and aminium[6,20] CIMS. While versatile and sensitive, these reagents are reactive, hazardous, and difficult to control, limiting their applicability. Müller et al.[21] have developed a novel low-pressure ammonium generation method that does not require the provision of ammonia, reducing the risks related to corrosion and toxicity. Still, the method does not fully meet the requirements for accurate and sensitive measurements. One of the limiting factors for the ammonium ionization scheme is the small size of the primary ion, which presents challenges related to ion transmission in the mass spectrometer, limiting the control and quantification capabilities of these CI systems.[22] In addition, the common method of providing ammonia in an aqueous solution is prone to drift, affecting the primary ion distribution and consequently altering the ionization regime.[19,23] Despite these limitations, ammonium CIMS garnered significant interest due to its ability to cluster with a wide range of compounds, providing complementary capabilities to conventional PTR-MS and negative mode CIMS. Motivated by these challenges and the need for a holistic analysis of gas-phase species, we set out to find a better alternative for positive mode ion attachment ionization targeting SVOCs, in particular moderately polar, lowly oxygenated, and basic compounds. The result of this exploration is the discovery of the uronium chemical ionization.

Urea ($NH_2C(O)NH_2$), is a simple yet remarkable organic compound, known for its biological, chemical, and industrial relevance. Urea became the first organic compound synthesized from inorganic substances by Friedrich Wöhler[24] in 1828, challenging the vitalism theory of organic chemistry and marking the advent of modern organic synthesis.[25] Urea is a well-known hydrogen bond donor that forms strong eutectic mixtures with a variety of compounds.[26] Structurally, urea is composed of two amino groups ($-NH_2$) attached to a central carbonyl group (C=O), a configuration that imparts high polarity and the ability to form hydrogen bonds. This molecular arrangement renders urea highly soluble in water, facilitating its natural occurrence in biological systems as the principal nitrogenous waste product of protein metabolism in mammals. Synthesized in the

liver, it provides a non-toxic mechanism for ammonia excretion, underscoring its critical role in maintaining nitrogen balance in living organisms.[27]

To the best of our knowledge, despite its emblematic role in science and nature and its favorable electronic structure, urea has never been tried as a CIMS reagent. The main challenge to overcome in the current work was to produce a sufficient gas-phase concentration of urea, a compound with negligible vapor pressure. The solution we found was x-ray desorption of solid-phase urea at room temperature. This novel method allowed us to create a sufficient number of uronium cations to act as CI reagent ions in a controlled and sustainable manner. To explore the suitability of uronium as a CI reagent we conducted a series of experiments to determine the sensitivity and stability of ionization reactions to a range of chemical compounds in varied humidities. Experiments were supported by quantum chemical studies to elucidate these reactions from a theoretical perspective. To explore the complementarity of the uronium to other CI reagents we performed series of VOC oxidation experiments using Multi-Pressure Chemical Ionization Mass Spectrometry (MPCIMS).[7] To validate the applicability of the method for the detection of ammonia in ambient air measurements, we performed a side-by-side comparison with a dedicated quantum cascade tunable infrared laser differential absorption spectrometer (QC-TILDAS, Aerodyne Research Inc.) widely used for quantification of atmospheric ammonia.[28]

Methods

Instrumentation

This study uses a multi-scheme chemical ionization inlet 2 (MION2, Karsa Ltd.) operating at ambient pressure[29,30] coupled to an Orbitrap Exploris 120 (Thermo Fisher Scientific Inc.) mass spectrometer[31] with a nominal mass resolution of 120,000. In brief, the MION2 inlet generates ions off-axis in a dedicated volume. Here we introduce a novel method for the production of reagent ions from solids (patent application submitted).

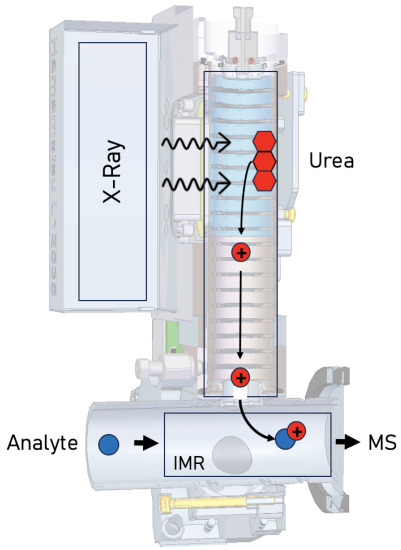

Figure 1: Setup for the uronium generation from solid urea by x-ray desorption and transfer of uronium into the ambient pressure ion-molecule reactor of the MION2 inlet.[30]

Figure 1 shows the geometry of the way solid urea was provided to the ionization volume. High-purity urea (VWR Chemicals, analytical reagent grade) is deposited into a custom-made holder (polyether ether ketone, PEEK) which is placed between MION2 electrodes exposing it to x-rays. The physical process of how urea is understood to sublimate is discussed in the Results and Discussion section. An electric field transports the ions into the ambient pressure ion-molecule reactor (IMR). The reagent gas in the ionized volume is kept apart from the sample gas by auxiliary gas flows. The reaction time within the IMR is approximately 25 ms. The sample gas then enters the Orbitrap mass spectrometer through a heated capillary (inner diameter 0.58 mm, length 58 mm). The capillary temperature was kept at 300 °C. Data were analysed with the Orbitool software package.[32] For VOC oxidation experiments, the ionization schemes were cycled between uronium ($NH_2C(O)NH_3^+$), nitrate (NO_3^-), and fluoranthenium ions($C_{16}H_{10}^+$) to assess the complete gas-phase product distribution.[7]

Long-term stability of the ionization method was assessed on a TD-APCI-TOF system simi-

lar to the one described here,[33] where the ionization unit was updated with a MION2 uronium source.

Independent ammonia measurements were performed using a quantum cascade tunable infrared laser differential absorption spectrometer (QC-TILDAS, Aerodyne Research Inc.)[28,34–36] which leverages quantitive knowledge of the ammonia absorption cross section to determine accurate concentrations.

Measurement data

This study generated data for calibration purposes, as well as data from laboratory flow reactor experiments aiming at α-pinene and DMS oxidation products, and observations from ambient field measurements.

The sensitivity of uronium for the detection of a number of compounds was determined in a set of calibration experiments that used a liquid calibration unit (LCU, Ionicon Analytik[37]). In the apparatus, dilute aqueous analyte solutions are sprayed into a heated chamber (110 °C) and carried by a carrier flow (1 lpm) into the main sample flow (20 lpm). Solutions were prepared in water, to avoid potential interferences from solvents such as e.g. methanol. Multi-point calibrations were carried out under varying degrees of humidification, from dry (RH< 5%) up to 80% relative humidity, and dosing levels varying by up to a factor of 30 (Fig. S1).

To create a spectrum of compounds with variable degree of oxidation, qualitative α-pinene oxidation experiments were carried out in a flow tube reactor (reaction time 6 s) under near-ambient conditions. A-pinene vapors were obtained by bubbling inert nitrogen through a liquid reservoir. Ozone was generated from synthetic air via UV light irradiation.

DMS oxidation experiments employed the same flow tube apparatus as the α-pinene experiments. DMS was dosed from a bottle (Air Products, 100 ppmv). Ethylene was added as dry OH source, and ozone was generated from synthetic air via UV light irradiation.

To evaluate the quantification capabilities under ambient conditions, we performed a side-by-side comparison with a dedicated ammonia instrument (QC-TILDAS) that passed by the institute. Ambient air was sampled to the uronium CIMS through a makeshift inlet (4 m long 10 mm inner diameter PTFE tubing) from the window of a laboratory located in the suburbs of Helsinki, Finland. At the end of the ambient measurements, both instruments sampled indoor (laboratory) air for a few hours, during which ammonia was also evaporated from a cloth to explore the response to higher concentrations.

Quantum chemical calculations

To explore the energetics of uronium ionization, several calculations were performed. The stabilities of ionic adducts of compounds listed in Table S1 with protonated urea ($CO(NH_2)_2H^+$) along with their respective tendencies to protonate, were examined using computational quantum chemical methods. A systematic conformational search was done using the MMFF molecular mechanics method in the Spartan '24 program (Wavefunction, Inc). Single-point energies were computed at the B3LYP/6-31+G* level[38–40] for all conformers using Spartan '24, and those within 5 kcal mol^{-1} in electronic energies of the lowest-energy conformer were considered for geometry optimizations. Geometry optimizations were first carried out at the B3LYP/6-31+G* level of theory and subsequently at ωB97X-D/6-31+G* (with frequency calculations)[41] for the conformers within 2 kcal mol^{-1} in electronic energies of the lowest-energy conformer. The energies of the lowest energy conformers were further refined at the DLPNO-CCSD(T)/def2-QZVPP level of theory. These geometry optimizations and frequency calculations were performed with the Gaussian 16 program,[42] while the ORCA 5.0.3 program[43] was used for DLPNO-CCSD(T) calculations.

As the hydrogen bonding sites are less obvious for the iodine-containing systems, a different approach was adopted to find their lowest energy clusters with uronium. The partial atomic charges for all iodine molecules and uronium were calculated with Gaussian 16 using the Pop=MKUFF keyword at the M062X/aug-

cc-pVTZ-(PP) level of theory. Iodine pseudopotentials were taken from the EMSL basis set library.[44,45] The atomic charges were then used for conformational sampling where the molecules were treated as rigid (intramolecular bonds and angles between bonds remain fixed) using the Artificial Bee Colony (ABC) algorithm implemented in the ABCluster program.[46–48] The following values were used for key parameters, $pop = 1000$, $gen = 100$, $-lm = 3000$. The resulting structures were then first optimized using semiempirical xTB method with "vTight" criteria.[49–51] The structures were then filtered to remove duplicates, as described in Kubečka et al.[47]. The resulting structures were first optimized at the M062X/SDD level of theory, and then at the M062X/aug-cc-pVTZ-PP level of theory on the subset of molecules within 5 kcal mol^{-1} of the lowest energy geometry in relative electronic energies. Finally, the energies of the lowest energy molecules were refined at the DLPNO-CCSD(T)/def2-QZVPP level of theory using ORCA program, which were used to calculate the cluster binding enthalpies.

Results and discussion

Generation of uronium ions

The saturation vapor pressure of urea is very low, at room temperature only about 10^{-8} atm (Fig. S5). Experimentally, uronium ions are observed only if some of the (solid) urea is illuminated by the x-ray charger (Fig. 1). Providing urea vapors conventionally from a reservoir of solid urea in an external reagent vial does not create any uronium signal, not even if the length of lines are minimized and ample time (one week) is dedicated for conditioning. On the other hand, if urea is introduced into a clean MION2 ion source and exposed to x-rays, the uronium signal appears instantaneously.

The exact mechanism by which urea sublimates to the gas phase is not clear, e.g., it is not clear whether neutral urea, uronium, or urea radicals evaporate. The enthalpy of sublimation of urea is approximately 95 kJ mol^{-1},

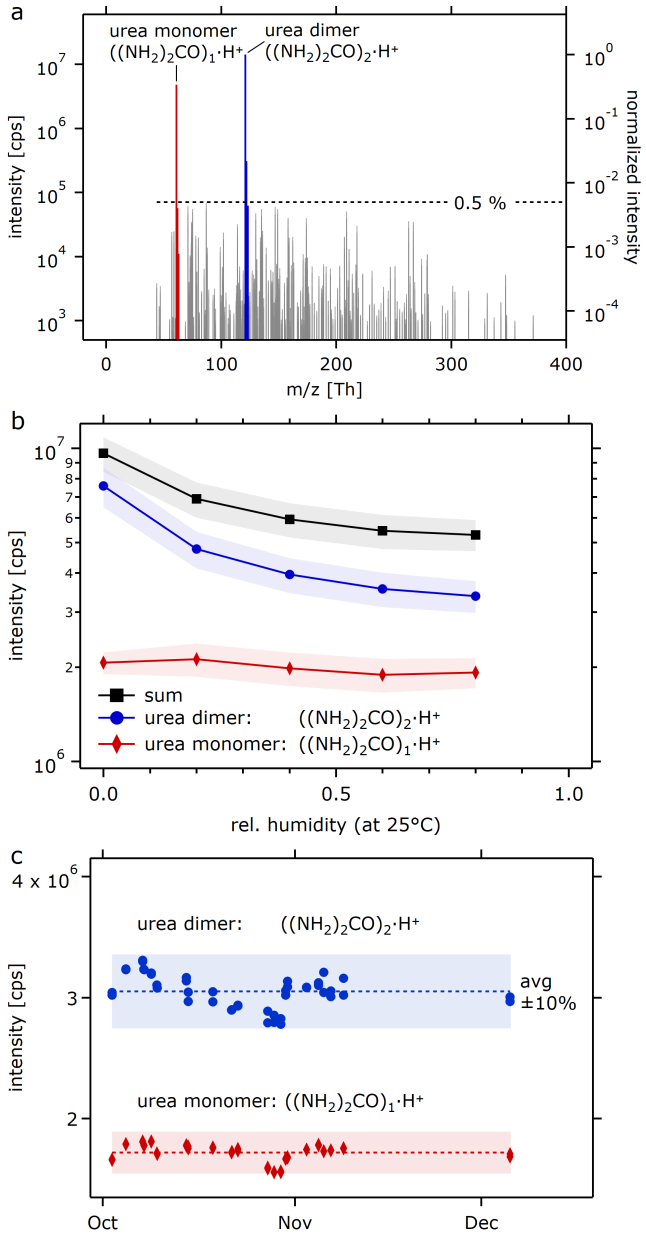

Figure 2: Cleanliness of uronium spectrum in absence of analyte (a, note the logarithmic intensity axis), sensitivity of reagent ion intensities to humidity changes (b), and stability of reagent ion provision over 2 months (c).

or 1 eV.[52] X-ray ionization kicks out electrons from their orbital. Relaxation of the atom to a lower electronic state releases energy (typically multiple eV) for evaporation to occur.[53–56] This is similar to Matrix-assisted laser desorption/ionization (MALDI), although the exact mechanism of volatilization and charging remain unknown.[57] We conclude that x-ray irradiation is required to induce significant sublimation of urea and the generation of uronium ions.[58,59]

We tested the approach to generate reagent ions from solids different than urea. The x-ray irradiation of ammonium nitrate salts also produces nitrate ions.[53] Here, the relative abundance of the nitrate dimer appears to be lower than when nitrate is formed from the irradiation of nitric acid vapors, provided from a liquid reservoir. At the same time, the intensity of the monomer ion was enhanced. This is consistent with a lower effective vapor concentration of nitric acid. The shifted distribution of the reagent ion using x-ray desorption might be exploited to enhance the sensitivity of nitrate chemical ionization to specific compound classes.[15] The mechanism of ion production from a solid precursor substance appears to be not limited to urea, and is warranted to be explored further.

Figure 2a shows the mass spectrum in the absence of analytes. Uronium and the urea–uronium cluster are the only dominant peaks. The observation of the dimer and oligomers is similar to that of other ionization approaches (NO_3^-, Br^-, etc.). The uronium–water peak was only observed at trace intensities at high RH (1000 cps or 10^{-4} ncps at 80% RH). This is consistent with a relatively low binding enthalpy between uronium and water (see below the theoretical analysis). The abundance of contaminant peaks is low, with contaminants not exceeding $5 \cdot 10^{-3}$ relative intensity (Fig. 2a) when analytical grade urea is used.

The sensitivity of the abundance of reagent ions to changes in humidity is shown in Fig. 2b. The abundance of the monomer is essentially constant. The abundance of the dimer decreases by approximately 50% when going from dry to wet conditions (80% RH). Between 20% and 80% RH the decrease is only 20%. The exchange reaction $U \cdot U \cdot H^+ + H_2O \longrightarrow U + U \cdot H_2O \cdot H^+$ (here, U denominates urea) is energetically not favorable (enthalpy difference 14.6 kcal mol^{-1}) but still relevant given the sheer abundance of water.

Figure 2c shows the remarkable long-term stability of uronium generation over more than 2 months. Without any retuning or resupply of reagent, neither the monomer nor the dimer abundance deviated more than 10% from the average. The result is a testament to the low evaporation rate, even in the presence of constant x-ray irradiation. The robust operation without the need for daily or even monthly maintenance should not only facilitate easier deployments but — by introducing less changes — also improve the quality of acquired data.

Theoretical calculation results

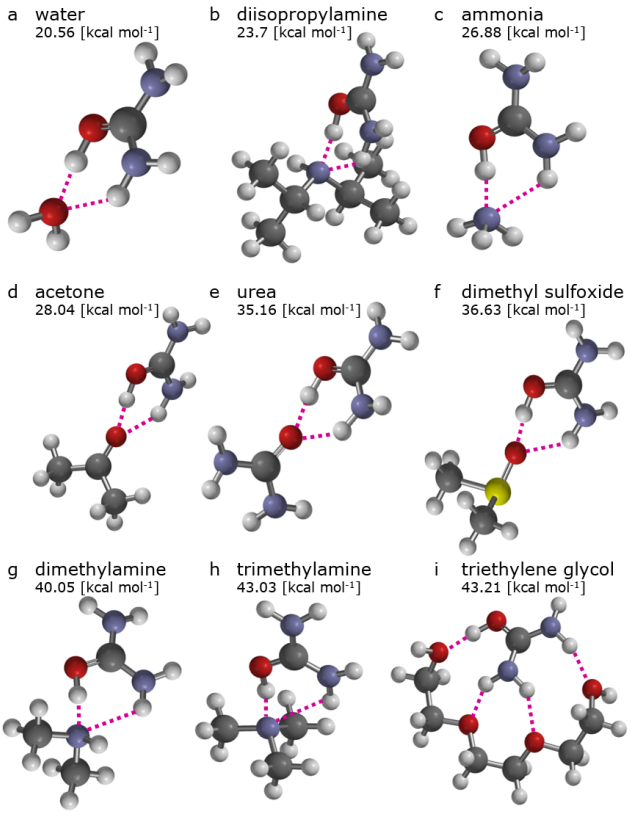

Figure 3: Geometries of clusters between uronium and selected analytes.

Figure 3 shows the cluster geometries for selected compounds containing different functional groups. The associated binding enthalpies are shown in Fig. 4 and tabulated

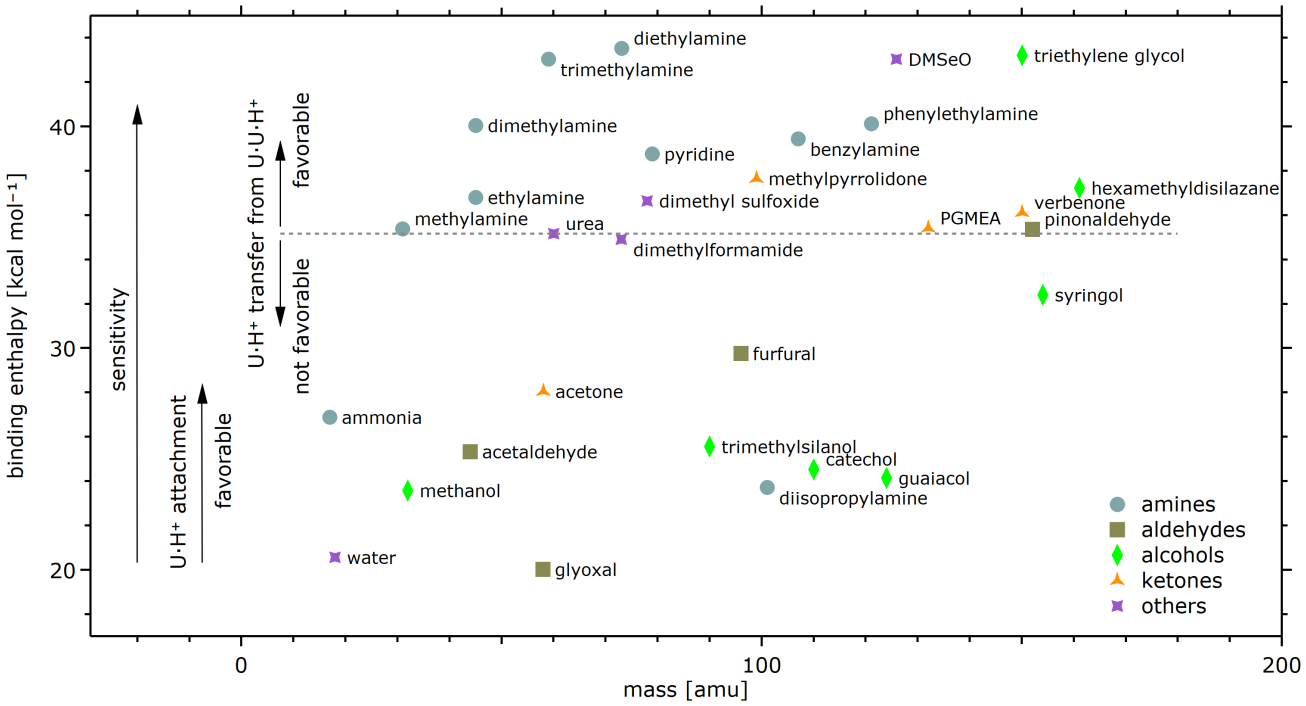

Figure 4: Calculated binding enthalpies for the formation of analyte–uronium clusters for compounds of different classes. Uronium transfer from the protonated urea-dimer ion is energetically favorable for enthalpies larger than 35.16 kcal mol^{-1}. The abbreviations refer to the following compounds: U: urea; PGMEA: propylene glycol methyl ether acetate; DMSeO: dimethyl selenoxide.

in Table S1. The protonation of urea occurs preferentially at the carbonyl group as the resulting cation is 16.02 kcal mol^{-1} lower in enthalpy compared to the cation with the proton on the nitrogen atom. The calculated proton affinity is 209.85 kcal mol^{-1} (compare literature value of 208.8 kcal mol^{-1} [60] and an estimated 1.6 kcal mol^{-1} error margin for the DLPNO-CCSD(T) method in predicting binding enthalpies[61]) and the dipole moment is 2.34 D – ammonium, in contrast, does not possess a net dipole moment. The most stable analyte-uronium cluster geometries contain hydrogen bond interactions from the carbonyl and at least one amino group of uronium. Analytes with multiple polar functional groups may exhibit interactions to multiple groups, e.g., triethylene glycol (Fig. 3), syringol, or glyoxal.

The interaction of uronium connected to two functional groups distinguishes it from e.g. ammonium, where only one significant interaction is established. The affinities of uronium to form a cluster are generally slightly stronger than those of ammonium (Table S1 and Xu et al.[23]), due to the higher electronegativity of oxygen compared to nitrogen. As a result, uronium clusters tend to be more stable and protonation by uronium is less likely.

Small molecular clusters with less than about 8 atoms are likely not efficiently collisionally stabilized during ionization, leading to lower instrument sensitivities despite strong binding enthalpies.[17,62] For example, the chemical ionization of IO by bromide or nitrate is not as efficient as that of e.g. sulfuric acid.[63] The substantial number of atoms of uronium should make it a better reagent ion to detect small molecules like IO. However, the calculated binding enthalpies of IO and other iodine oxidation products were found to be unfavorably low (Table S1).

Figure 4 shows the calculated enthalpies for different clusters against fragmentation into uronium and the analyte. The enthalpies are shown here because they were shown to better predict ionization efficiencies than free energies.[62] Higher binding enthalpies generally lead to higher chances of ionization, as long as the

system size allows sufficient dissipation of energy.[17,62]

The enthalpy for uronium to cluster with urea to form the UUH^+ dimer ion (35.16 kcal mol^{-1}, Fig. 3e) influences to what extent the dimer participates in the formation of analyte–uronium clusters. Due to the strong binding enthalpy of the uronium–urea cluster, it forms stable reagent ion dimers under our experimental conditions. The ionization of an analyte then happens through a ligand exchange reaction, where analyte–uromium clusters with binding enthalpies in excess of 35.16 kcal mol^{-1} are more efficiently ionized than the more weakly bound clusters. Importantly, the binding enthalpy between uronium and water is relatively low (20.56 kcal mol^{-1}), such that the reagent ion is not strongly interacting with water, and humidity sensitivities are minor.

Another route for newly formed clusters is the fragmentation into neutral urea and protonated analyte. This is more likely for compounds with high proton affinity. The energetics of the uronium proton transfer reactions were determined for different compounds and are illustrated in Fig. S6, showing trends and outliers within different compound classes. The extent to which the fragmentation occurs depends on the energies, the distribution of energy within the cluster, and the dissipation of excess energy to the bath gas. The initial interaction between uronium and analyte determines the overall likelihood for ionization.

The trend of increasing binding enthalpies for e.g. the amines is the combined result of the changing dipole moment and the ability of the larger molecules to adapt energetically favorable configurations. In case of diisopropylamine (Fig. 3b), the two methyl groups with net positive charge provide steric hindrance and make the uronium ion bond with the NH group less favorable. However, the proton affinity of diisopropylamine is very high (232.5 kcal mol^{-1} [64]), resulting in excellent detection in its protonated form.

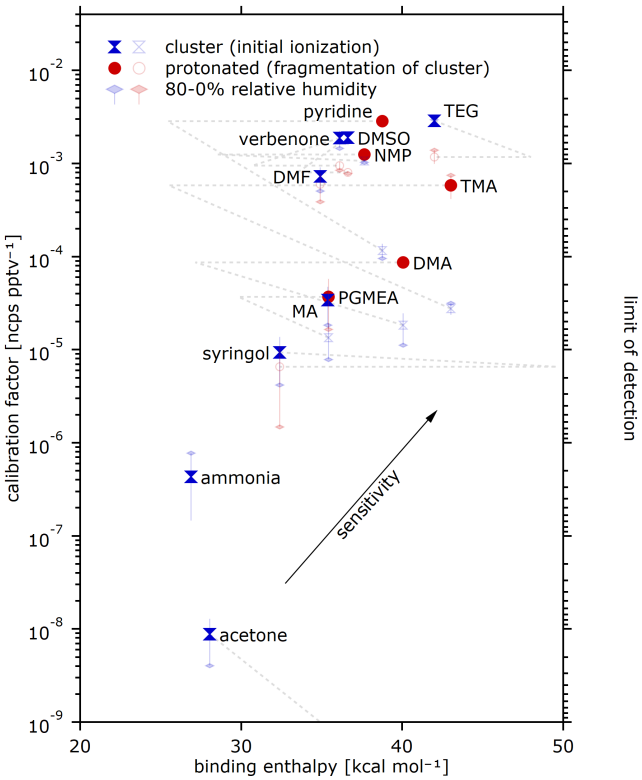

Figure 5: Sensitivity of uronium CIMS to detect different analytes. The left axis shows the calibration factors [ncps ppt^{-1}], where ncps is the relative intensity of the product ion to the summed intensity of the reagent ions. The right axis illustrates estimated limits of detection, i.e., the volume mixing ratio corresponding to a respective peak signal of 100 cps (not considering the instrument baseline). The abbreviations refer to the following compounds: DMSO: dimethyl sulfoxide; DMF: dimethyl formamide; NMP: N-methyl-2-pyrrolidone; TEG: triethylene glycol; TMA: trimethylamine; DMA: dimethylamine; PGMEA: propylene glycol methyl ether acetate; MA: methylamine.

Calibration results

Figure 5 shows the measured calibration factors derived from the multi-point calibrations under varied humidity (see Methods) for the different compounds on the left axis, while the right axis indicates the respective limits of detection, estimated as the volume mixing ratio corresponding to the assumed lowest detectable peak intensities of 100 cps. All signals are normalized by the sum of the uronium monomer and dimer ion. The abscissa is the calculated binding enthalpy of the uronium–analyte cluster, the energy associated with the first interaction between the analyte and uronium. The markers indicate the calibration factor for detection as cluster (blue hourglass) or protonated analyte (red circle). The dashed grey lines connect the two respective experimental calibration factors via the binding enthalpy of the cluster against fragmentation into the protonated analyte and neutral urea. The uronium-analyte clusters tend to fragment into the protonated analyte and neutral urea if energetically favorable. In this case, the detection of a target compound via the protonated analyte yields better sensitivity. For example, the fragmentation of the uronium–trimethylamine cluster into urea and trimethylaminium is favorable by about 15 kcal mol^{-1}, and trimethylamine is mostly detected as trimethylaminium. Vice versa, triethylene glyocol is mostly detected as cluster with uronium. As expected from theory, higher sensitivities are found for larger binding enthalpies.[62] Acetone is detected with a surprisingly low sensitivity, which we speculate to originate from some sort of reactive interaction between acetone and urea.[65]

Figure 5 further illustrates the humidity sensitivity of the calibration factors, a known feature to different ionization schemes. In case of ammonia, one compound exhibiting a more pronounced sensitivity, the calibration factor varies by a factor 5, requiring proper account of changes in humidity during measurements. Most of the other compounds tested exhibit a calibration factor that varies not more than a few 10%. While a clear trend is lacking in the limited set of compounds tested, it seems plausible that water could help in the ionization of small molecules via sacrificial cooling.[66]

Table 1 summarizes the experimental sensitivities. The detection limits attainable with uronium are in the parts per trillion per volume (pptv) to parts per quadrillion per volume (ppqv) range, as combination of uronium's favorable tendency to interact with the analytes and the maximized opportunity for ionization to occur during the relatively long reaction time (approximately 25 ms) under ambient pressure. For this reason, these detection limits are of similar magnitude as e.g. those attainable for sulfuric acid using a nitrate CIMS. In absolute terms, at maximum sensitivity, as few as 10 attomoles are required to produce 100 counts, the lowest detectable signal.

The sensitivity to DMSO was characterized to be very high, with respective detection limits in the ppqv range. This is particularly interesting in light of the importance of atmospheric DMS oxidation, which, by forming sulfuric acid, is a globally important driver of particle formation. The details of the oxidation mechanism, e.g., the branching of pathways, are still being investigated.[67,68] Beyond DMSO, clusters of uronium with DMSO2 were apparently also observed in exploratory flow tube experiments of DMS oxidation. However, accurate calibration factors could not be produced due to the lack of calibration standards.

The sensitivity to amines is likewise favorably high, both for detection as cluster with uronium or as protonated molecule. In our oxidizing atmosphere that promotes the formation of acids, amines are important to atmospheric aerosol particle formation.[69,70] Ammonia, the isolated functional amino group, is only detected as cluster with uronium, due to the minute mass of ammonium. The amines (larger than methylamine) are also detected in their protonated form. It might be considered a happy coincidence that the sensitivity to the tested amines is approximately inverse to their atmospheric abundance, i.e., the sensitivity to the relatively common ammonia is lower than e.g. dimethylamine. One could also argue that less interacting, more volatile gases should occur at higher abundance. Regardless, the trend in sensitivity,

Table 1: Experimental calibration factors c and detection limits λ for different compounds. Here, c_0 is the calibration factor under dry conditions, γ the coefficient of relative humidity sensitivity, such that for a given humidity $\phi \in [0, 1]$ the calibration factor is $c = c_0(1 + \gamma\phi)$ [ncps pptv^{-1}]. λ_{100} [pptv] is the detection limit equivalent to 100 cps signal, the approximately lowest signals still detectable. λ_{BL} [pptv] is the detection limit equivalent to the instrument background (if present). λ_{SDEV} [pptv] is the detection limit that corresponds to three times the standard deviation of a the instrument background (if present).

		cluster					protonated				
target	sum formula	c_0	γ	λ_{100}	λ_{BL}	λ_{SDEV}	c_0	γ	λ_{100}	λ_{BL}	λ_{SDEV}
ammonia	NH_3	1.5E-7	4.28	23	2300	350					
MA	CH_3NH_2	4.8E-5	-0.62	0.29	0.78						
DMA	$(CH_3)_2NH$	2.5E-5	-0.55	0.54	1.4	0.88	8.2E-5	0.12	0.12	0.19	0.051
TMA	$(CH_3)_3N$	2.4E-5	0.33	0.36	1.0	0.21	4.2E-4	0.79	0.017		
pyridine	C_5H_5N	1.4E-4	-0.30	0.086	0.59	0.45	2.6E-3	0.15	0.0035	0.48	0.10
DMF	C_3H_7NO	9.1E-4	-0.45	0.014	0.86	0.19	7.8E-4	-0.50	0.017	0.91	0.32
DMSO	C_2H_6OS	2.1E-3	-0.19	0.0053	0.023	0.0057	8.2E-4	-0.05	0.012	0.027	0.012
syringol	$C_8H_{10}O_3$	1.4E-5	-0.70	1.1	2.5	2.7	1.1E-5	-0.86	1.5	5.6	1.7
verbenone	$C_{10}H_{14}O$	2.3E-3	-0.36	0.0053	0.013	0.0051	1.0E-3	-0.18	0.011		
PGMEA	$C_6H_{12}O_3$	1.9E-5	-0.59	0.74	1.9		5.8E-5	-0.71	0.27		
acetone	C_3H_6O	1.3E-8	-0.69	1100	2800	3800	9.3E-11	-0.40	130000		
TEG	$C_6H_{14}O_4$	2.8E-3	0.05	0.0035	0.083	0.026	9.9E-4	0.39	0.0085	0.10	0.053
NMP	C_5H_9NO	1.1E-3	-0.07	0.0094	0.09	0.044	1.3E-3	-0.05	0.008	0.11	0.043

in line with binding enthalpies, is welcome.

The chemical ionization of amines has been previously accomplished by proton-transfer reactions[71–74]. Nowak et al.[75],[76] pioneered the detection of ammonia by ethanol CIMS[77], and developed an improved CIMS employing acetone dimers for the detection of ammonia.[78,79] Protonated ethanol or acetone ions were later also used as ionization reagents to also selectively detect other high proton affinity base compounds (e.g. amines and ammonia[80,81]). Sipilä et al.[82] explored dosing sulfuric acid in an NO_3^- CIMS for the detection of ammonia and amines via clustering with the bisulfate ion. However, operational complexities of these prior CIMS approaches have hampered their adoption by the general atmospheric CIMS community. We believe that the robust operation of the uronium CIMS facilitates routine measurements of amines, thereby better constraining atmospheric particle formation.

Ambient NH_3 measurements

Figure 6 demonstrates the remarkable potential of uronium CIMS to quantify even low abundances of ammonia in atmospheric measurements. In absence of a dedicated NH_3 free overflow system, the instrument background of the CIMS measurement was accounted for by subtracting the lowest normalized signal intensity observed during the observations. The intensity of the detected peak was scaled by a humidity-dependent calibration factor ($8.6 \cdot 10^{-7}$ ncps pptv^{-1} for the moist ambient measurements and $6.2 \cdot 10^{-7}$ ncps pptv^{-1} for the drier indoor measurements). The thusly baseline corrected and scaled time series (1 min averages) are shown in Figure 6 (red markers) along with the QC-TILDAS time series. Volume mixing ratios ranged from a few 10s of pptv to single ppbv during the ambient measurements, to 3 ppbv indoor VMR and peaking at around 100 ppbv in the spiked experiment.

The ratio of VMRs measured by the uronium CIMS and QC-TILDAS is generally unity within a maximum deviation of a few 10%. The fairly long CIMS inlet line used for the comparison limits the temporal response to changes in NH_3 abundance. Differences in line conditioning hamper the direct comparison of the data during the transients of the laboratory ex-

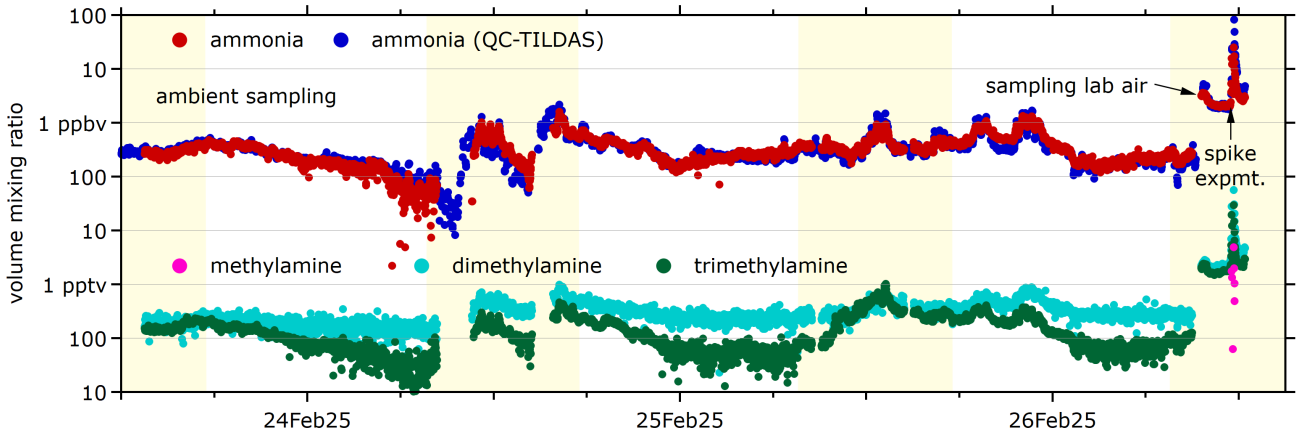

Figure 6: Ammonia and amine abundance in ambient and laboratory air. On Feb 26, ammonia was evaporated into the laboratory to test the response to high VMR. The uronium CIMS derived ammonia time series agrees well with the QC-TILDAS-determined time series. Methylamine is only detected during the spiking experiment, likely as impurity of the dosed ammonia.

periment, but it appears that there is a good correlation across at least 2 orders of magnitude in abundance, from several 10s of pptv to several ppbv. Determining the NH_3 instrument baseline was hampered by the absence of a dedicated ambient sampling inlet and lack of ammonia scrubber, and would be required for the accurate determination of absolute ammonia concentrations in independent deployments of a uronium CIMS that lack the luxury of a reference instrument. Determining the NH_3 baseline is notoriously difficult, reflected in the fact that QC-TILDAS is dedicating 30% of the time to assessing the instrument background, sampling from zero air every 15 min. Overall, the comparison shows that uronium CIMS can be used to measure atmospheric bases, and given even higher sensitivities, it should provide an excellent handle on other amines.

Figure 6 further shows the timeseries of methylamine (CH_3NH_2), C_2H_6NH (dimethylamine), and C_3H_9N (trimethylamine). The time series were scaled with the laboratory derived calibration factors and corrected for the respective instrument background by subtracting the lowermost value of the time series, equivalent as for ammonia. The thusly determined volume mixing ratios are in the sub-pptv range for ambient measurements, and pptvs for indoor air. Methylamine is only detected during the spike experiments, somewhat in contrast to the expectation of observing it at abundances higher than other amines.[69,83] The separation of isomers (e.g., by gas chromatography) would be required to positively attribute the detected peaks of the larger amines to the different isomers, but should be possible given the very low detection limits.

Laboratory α-pinene experiments

Figure 7 shows the capability of uronium to ionize organic molecules in the α-pinene oxidation experiments relative to nitrate and fluoranthenium ionization in a Kendrick and a van Krevelen diagram. Nitrate chemical ionization is well known to be selective to highly oxygenated compounds.[84] Low-pressure positive ionization (e.g. PTR) creates sensitivity to lowly or non-oxygenated volatile compounds. Here, fluoranthenium was used to detect α-pinene, the non-oxidized precursor and other reaction products.[7] Uronium positive mode at ambient pressure bridges the gap between these two schemes and extends the sensitivity to lowly oxygenated compounds. Figure 7 reinforces that the chemical variety of trace gases requires the use of different ionization schemes across polarity and pressure to attain comprehensive detection sensitivity.

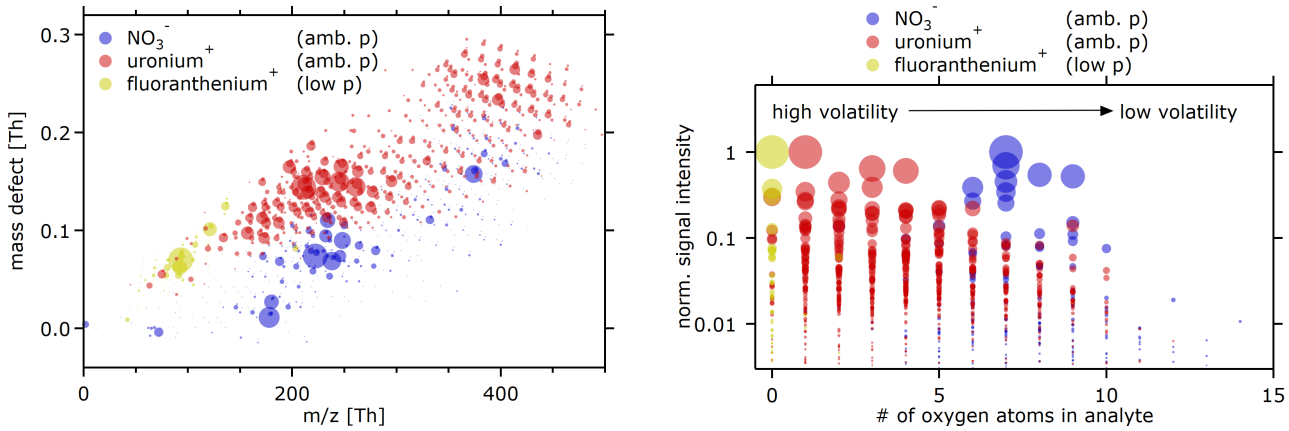

Figure 7: Mass-defect figure (masses and mass defects of the compounds without the reagent) and intensities of compounds with varying number of oxygen atoms detected during α-pinene oxidation experiments using nitrate, uronium and fluoranthenium ionization (blue, red, yellow markers, respectively). The marker area is proportional to the normalized intensity in each mode. Multiple ionization schemes are needed to create sensitivity to the chemically varied spectrum of volatile (precursor) gases and oxidized reaction products.

Conclusions

Uronium CIMS and means of providing reagent precursor via x-ray desorption of solids is a new approach for sensitive analysis of complex gas mixtures. We inspected uronium's applicability as a reagent ion through series of laboratory experiments, featuring multi-point calibrations to several compounds of interest in wide range of humidities. The interpretation of the experimental results was supported by theoretical study including quantum chemical computations of reaction thermodynamics between uronium and analytes under investigation. To assess the complementarity of uronium to low-pressure and negative mode ionization schemes we conducted series of α-pinene and DMS oxidation experiments yielding a wide range of reaction products of different volatilities using an MPCIMS system. To test the applicability of uronium CIMS for the quantification of trace gases in demanding applications, we conducted ambient measurements alongside QC-TILDAS, a standard technique for atmospheric ammonia measurements.

The ability of uronium to selectively form strong clusters and the resulting applicability in ambient-pressure IMRs create excellent sensitivities to several key compound classes. The exceptional sensitivity of uronium CIMS to basic compounds including ammonia and amines — compounds that are notoriously difficult to measure — facilitates the enhanced and more routine assessment of bases in ambient CIMS deployments. The sensitivity range synergizes with that of low-pressure positive and ambient-pressure negative ionization, enabling a near-complete coverage with just one mass spectrometer.[6,7]

Another benefit of uronium ionization over similar approaches, e.g., ammonium ionization, is the alleviation of several operational challenges, specifically the robust and stable provision of ions, the possible normalization due to its moderate mass, and the easy and safe operation. Because of the negligible vapor pressure, contaminating the instrument with the reagent, a common hazard with nitric acid and ammonia, is also obviated.

In addition, we have successfully tested the x-ray irradiation of ammonium nitrate, a solid with a vapor pressure similar to that of urea,[85,86] for the generation of nitrate reagent ions. Lower nitric acid and higher nitrate concentrations might allow optimizing the sensitivity of nitrate CIMS to a broader range of compounds.[15]

Overall, we believe that the method of x-ray reagent desorption in general, and uronium

chemical ionization in particular, can improve the operability of CIMS, enhance its performance for gas-phase analytics in atmospheric and environmental research, and pave the way towards its standardization and wider use in industrial applications.

Acknowledgement This study was supported by the Finnish Research Impact Foundation and Research Council of Finland (353836, 356134, 358066, 364223, 346370, 346373, 355966). This project has received funding from the European Research Council under the European Union's Horizon 2020 research and innovation programme under Grant No. 101002728. We acknowledge ACTRIS CiGas-UHEL (Centre for Reactive Trace Gases In Situ Measurements, University of Helsinki, Academy of Finland (329274)) for providing support to instruments.

Declaration of Competing Interests

Some of the authors work for Karsa Ltd., the manufacturer of the MION2 inlet and related mass spectrometry systems.

References

(1) Hayeck, N.; Temime-Roussel, B.; Gligorovski, S.; Mizzi, A.; Gemayel, R.; Tlili, S.; Maillot, P.; Pic, N.; Vitrani, T.; Poulet, I.; Wortham, H. Monitoring of organic contamination in the ambient air of microelectronic clean room by proton-transfer reaction/time-of-flight/mass spectrometry (PTR–ToF–MS). *International Journal of Mass Spectrometry* **2015**, *392*, 102–110.

(2) Vitucci, E. C. M.; Oladeji, O.; Presto, A. A.; Cannon, C. L.; Johnson, N. M. The application of PTR-MS and non-targeted analysis to characterize VOCs emitted from a plastic recycling facility fire. *Journal of Exposure Science & Environmental Epidemiology* **2024**,

(3) Taylor, A. J.; Beauchamp, J. D.; Langford, V. S. *Dynamic Flavor: Capturing Aroma Using Real-Time Mass Spectrometry*; ACS Symposium Series; American Chemical Society, 2021; Vol. 1402; Chapter 1, pp 1–16.

(4) Jia, Z.; Ong, W. Q.; Zhang, F.; Du, F.; Thavasi, V.; Thirumalai, V. A study of 9 common breath VOCs in 504 healthy subjects using PTR-TOF-MS. *Metabolomics* **2024**, *20*, 79.

(5) Zhang, W.; Xu, L.; Zhang, H. Recent advances in mass spectrometry techniques for atmospheric chemistry research on molecular-level. *Mass Spectrometry Reviews* **2023**,

(6) Cai, R.; Mikkilä, J.; Bengs, A.; Koirala, M.; Mikkilä, J.; Holm, S.; Juuti, P.; Meder, M.; Partovi, F.; Shcherbinin, A.; Worsnop, D.; Ehn, M.; Kangasluoma, J. Extending the Range of Detectable Trace Species with the Fast Polarity Switching of Chemical Ionization Orbitrap Mass Spectrometry. *Analytical Chemistry* **2024**,

(7) Shcherbinin, A.; Finkenzeller, H.; Mikkilä, J.; Kontro, J.; Vinkvist, N.; Kangasluoma, J.; Rissanen, M. From Hydrocarbons to Highly Functionalized Molecules in a Single Measurement: Comprehensive Analysis of Complex Gas Mixtures by Multi-pressure Chemical Ionization Mass Spectrometry. *Analytical Chemistry* **2024**,

(8) Frege, C. et al. Influence of temperature on the molecular composition of ions and charged clusters during pure biogenic nucleation. *Atmospheric Chemistry and Physics* **2018**, *18*, 65–79.

(9) Robinson, M. A.; Neuman, J. A.; Huey, L. G.; Roberts, J. M.; Brown, S. S.; Veres, P. R. Temperature-dependent sensitivity of iodide chemical ionization mass spectrometers. *Atmospheric Measurement Techniques* **2022**, *15*, 4295–4305.

(10) Hyttinen, N.; Otkjær, R. V.; Iyer, S.; Kjaergaard, H. G.; Rissanen, M. P.; Wennberg, P. O.; Kurtén, T. Computational Comparison of Different Reagent Ions in the Chemical Ionization of Oxidized Multifunctional Compounds. *The Journal of Physical Chemistry A* **2018**, *122*, 269–279.

(11) Pleil, J. D.; Hansel, A.; Beauchamp, J. Advances in proton transfer reaction mass spectrometry (PTR-MS): applications in exhaled breath analysis, food science, and atmospheric chemistry. *Journal of Breath Research* **2019**, *13*, 039002.

(12) Kari, E.; Miettinen, P.; Yli-Pirilä, P.; Virtanen, A.; Faiola, C. L. PTR-ToF-MS product ion distributions and humidity-dependence of biogenic volatile organic compounds. *International Journal of Mass Spectrometry* **2018**, *430*, 87–97.

(13) Li, H.; Almeida, T. G.; Luo, Y.; Zhao, J.; Palm, B. B.; Daub, C. D.; Huang, W.; Mohr, C.; Krechmer, J. E.; Kurtén, T.; Ehn, M. Fragmentation inside proton-transfer-reaction-based mass spectrometers limits the detection of ROOR and ROOH peroxides. *Atmospheric Measurement Techniques* **2022**, *15*, 1811–1827.

(14) Li, F.; Huang, D. D.; Tian, L.; Yuan, B.; Tan, W.; Zhu, L.; Ye, P.; Worsnop, D.; Hoi, K. I.; Mok, K. M.; Li, Y. J. Response of protonated, adduct, and fragmented ions in Vocus proton-transfer-reaction time-of-flight mass spectrometer (PTR-ToF-MS). *Atmospheric Measurement Techniques* **2024**, *17*, 2415–2427.

(15) Garmash, O.; Kumar, A.; Jha, S.; Barua, S.; Hyttinen, N.; Iyer, S.; Rissanen, M. Enhanced detection of aromatic oxidation products using NO3- chemical ionization mass spectrometry with limited nitric acid. *Environmental Science: Atmospheres* **2024**, *4*, 1368–1381.

(16) Sanchez, J.; Tanner, D. J.; Chen, D.; Huey, L. G.; Ng, N. L. A new technique for the direct detection of HO2 radicals using bromide chemical ionization mass spectrometry (Br-CIMS): initial characterization. *Atmos. Meas. Tech.* **2016**, *9*, 3851–3861.

(17) Lee, B. H.; Lopez-Hilfiker, F. D.; Mohr, C.; Kurtén, T.; Worsnop, D. R.; Thornton, J. A. An Iodide-Adduct High-Resolution Time-of-Flight Chemical-Ionization Mass Spectrometer: Application to Atmospheric Inorganic and Organic Compounds. *Environmental Science & Technology* **2014**, *48*, 6309–6317.

(18) Ehn, M. et al. A large source of low-volatility secondary organic aerosol. *Nature* **2014**, *506*, 476–479.

(19) Canaval, E.; Hyttinen, N.; Schmidbauer, B.; Fischer, L.; Hansel, A. NH4+ Association and Proton Transfer Reactions With a Series of Organic Molecules. *Frontiers in Chemistry* **2019**, *7*.

(20) Berndt, T.; Herrmann, H.; Kurtén, T. Direct Probing of Criegee Intermediates from Gas-Phase Ozonolysis Using Chemical Ionization Mass Spectrometry. *Journal of the American Chemical Society* **2017**, *139*, 13387–13392.

(21) Müller, M.; Piel, F.; Gutmann, R.; Sulzer, P.; Hartungen, E.; Wisthaler, A. A novel method for producing NH4+ reagent ions in the hollow cathode glow discharge ion source of PTR-MS instruments. *International Journal of Mass Spectrometry* **2020**, *447*, 116254.

(22) Riva, M.; Ehn, M.; Li, D.; Tomaz, S.; Bourgain, F.; Perrier, S.; George, C. CI-Orbitrap: An Analytical Instrument To Study Atmospheric Reactive Organic Species. *Analytical Chemistry* **2019**, *91*, 9419–9423.

(23) Xu, L.; Coggon, M. M.; Stockwell, C. E.; Gilman, J. B.; Robinson, M. A.; Breitenlechner, M.; Lamplugh, A.; Crounse, J. D.;

Wennberg, P. O.; Neuman, J. A.; Novak, G. A.; Veres, P. R.; Brown, S. S.; Warneke, C. Chemical ionization mass spectrometry utilizing ammonium ions (NH4+ CIMS) for measurements of organic compounds in the atmosphere. *Atmospheric Measurement Techniques* **2022**, *15*, 7353–7373.

(24) Wöhler, F. Ueber künstliche Bildung des Harnstoffs. *Annalen der Physik* **1828**, *88*, 253–256.

(25) Kinne-Saffran, E.; Kinne, R. K. H. Vitalism and Synthesis of Urea : From Friedrich Wöhler to Hans A. Krebs. *American Journal of Nephrology* **1999**, *19*, 290–294.

(26) Smith, E. L.; Abbott, A. P.; Ryder, K. S. Deep Eutectic Solvents (DESs) and Their Applications. *Chemical Reviews* **2014**, *114*, 11060–11082.

(27) Weiner, I. D.; Mitch, W. E.; Sands, J. M. Urea and ammonia metabolism and the control of renal nitrogen excretion. *Clinical Journal of the American Society of Nephrology* **2015**, *10*, 1444–1458.

(28) Ellis, R. A.; Murphy, J. G.; Pattey, E.; van Haarlem, R.; O'Brien, J. M.; Herndon, S. C. Characterizing a Quantum Cascade Tunable Infrared Laser Differential Absorption Spectrometer (QC-TILDAS) for measurements of atmospheric ammonia. *Atmospheric Measurement Techniques* **2010**, *3*, 397–406.

(29) Rissanen, M. P.; Mikkilä, J.; Iyer, S.; Hakala, J. Multi-scheme chemical ionization inlet (MION) for fast switching of reagent ion chemistry in atmospheric pressure chemical ionization mass spectrometry (CIMS) applications. *Atmos. Meas. Tech.* **2019**, *12*, 6635–6646.

(30) Finkenzeller, H.; Mikkilä, J.; Righi, C.; Juuti, P.; Sipilä, M.; Rissanen, M.; Worsnop, D.; Shcherbinin, A.; Sarnela, N.; Kangasluoma, J. Multiphysical description of atmospheric pressure interface chemical ionisation in MION2 and Eisele type inlets. *Atmospheric Measurement Techniques* **2024**, *17*, 5989–6001.

(31) Hauschild, J.-P. et al. A Novel Family of Quadrupole-Orbitrap Mass Spectrometers for a Broad Range of Analytical Applications. 2020; `https://doi.org/10.20944/preprints202006.0111.v1`.

(32) Cai, R.; Li, Y.; Clément, Y.; Li, D.; Dubois, C.; Fabre, M.; Besson, L.; Perrier, S.; George, C.; Ehn, M.; Huang, C.; Yi, P.; Ma, Y.; Riva, M. Orbitool: a software tool for analyzing online Orbitrap mass spectrometry data. *Atmospheric Measurement Techniques* **2021**, *14*, 2377–2387.

(33) Kangasluoma, J.; Mikkilä, J.; Hemmilä, V.; Kausiala, O.; Hakala, J.; Iakovleva, E.; Juuti, P.; Sipilä, M.; Junninen, H.; Jost, H. J.; Shcherbinin, A. Atmospheric pressure thermal desorption chemical ionization mass spectrometry for ultra-sensitive explosive detection. *Talanta* **2022**, *249*, 123653.

(34) McManus, J. B.; Shorter, J. H.; Nelson, D. D.; Zahniser, M. S.; Glenn, D. E.; McGovern, R. M. Pulsed quantum cascade laser instrument with compact design for rapid, high sensitivity measurements of trace gases in air. *Applied Physics B* **2008**, *92*, 387–392.

(35) Moravek, A.; Singh, S.; Pattey, E.; Pelletier, L.; Murphy, J. G. Measurements and quality control of ammonia eddy covariance fluxes: a new strategy for high-frequency attenuation correction. *Atmospheric Measurement Techniques* **2019**, *12*, 6059–6078.

(36) Pollack, I. B.; Lindaas, J.; Roscioli, J. R.; Agnese, M.; Permar, W.; Hu, L.; Fischer, E. V. Evaluation of ambient ammonia measurements from a research aircraft using a closed-path QC-TILDAS operated

with active continuous passivation. *Atmospheric Measurement Techniques* **2019**, *12*, 3717–3742.

(37) Fischer, L.; Klinger, A.; Herbig, J.; Winkler, K.; Gutmann, R.; Hansel, A. The LCU: versatile trace gas calibration. 6th International Conference on Proton Transfer Reaction Mass Spectrometry and its Applications Proceedings. 2013; pp 192–194.

(38) Becke, A. D. Density-functional thermochemistry. III. The role of exact exchange. *The Journal of Chemical Physics* **1993**, *98*, 5648–5652.

(39) Lee, C.; Yang, W.; Parr, R. G. Development of the Colle-Salvetti correlation-energy formula into a functional of the electron density. *Physical Review B* **1988**, *37*, 785–789.

(40) Frisch, M. J.; Pople, J. A.; Binkley, J. S. Self-consistent molecular orbital methods 25. Supplementary functions for Gaussian basis sets. *The Journal of Chemical Physics* **1984**, *80*, 3265–3269.

(41) Chai, J.-D.; Head-Gordon, M. Long-range corrected hybrid density functionals with damped atom–atom dispersion corrections. *Physical Chemistry Chemical Physics* **2008**, *10*, 6615–6620.

(42) Frisch, M. J. et al. Gaussian 16 Revision C.01. 2016.

(43) Neese, F.; Wennmohs, F.; Becker, U.; Riplinger, C. The ORCA quantum chemistry program package. *The Journal of Chemical Physics* **2020**, *152*, 224108.

(44) Kendall, R. A.; Dunning Jr., T. H.; Harrison, R. J. Electron affinities of the first-row atoms revisited. Systematic basis sets and wave functions. *The Journal of Chemical Physics* **1992**, *96*, 6796–6806.

(45) Dunning Jr., T. H. Gaussian basis sets for use in correlated molecular calculations. I. The atoms boron through neon and hydrogen. *The Journal of Chemical Physics* **1989**, *90*, 1007–1023.

(46) Kubečka, J.; Besel, V.; Neefjes, I.; Knattrup, Y.; Kurtén, T.; Vehkamäki, H.; Elm, J. Computational Tools for Handling Molecular Clusters: Configurational Sampling, Storage, Analysis, and Machine Learning. *ACS Omega* **2023**, *8*, 45115–45128.

(47) Kubečka, J.; Besel, V.; Kurtén, T.; Myllys, N.; Vehkamäki, H. Configurational Sampling of Noncovalent (Atmospheric) Molecular Clusters: Sulfuric Acid and Guanidine. *The Journal of Physical Chemistry A* **2019**, *123*, 6022–6033.

(48) Zhang, J.; Dolg, M. ABCluster: the artificial bee colony algorithm for cluster global optimization. *Phys. Chem. Chem. Phys.* **2015**, *17*, 24173–24181.

(49) Bannwarth, C.; Caldeweyher, E.; Ehlert, S.; Hansen, A.; Pracht, P.; Seibert, J.; Spicher, S.; Grimme, S. Extended tight-binding quantum chemistry methods. *WIREs Computational Molecular Science* **2021**, *11*, e1493.

(50) Bannwarth, C.; Ehlert, S.; Grimme, S. GFN2-xTB—An Accurate and Broadly Parametrized Self-Consistent Tight-Binding Quantum Chemical Method with Multipole Electrostatics and Density-Dependent Dispersion Contributions. *Journal of Chemical Theory and Computation* **2019**, *15*, 1652–1671.

(51) Pracht, P.; Caldeweyher, E.; Ehlert, S.; Grimme, S. A robust non-self-consistent tight-binding quantum chemistry method for large molecules. **2019**,

(52) Zaitsau, D.; Kabo, G. J.; Kozyro, A. A.; Sevruk, V. M. The effect of the failure of isotropy of a gas in an effusion cell on the vapor pressure and enthalpy of sublimation for alkyl derivatives of carbamide. *Thermochimica Acta* **2003**, *406*, 17–28.

(53) Aduru, S.; Contarini, S.; Rabalais, J. W. Electron-, x-ray-, and ion-stimulated decomposition of nitrate salts. *The Journal of Physical Chemistry* **1986**, *90*, 1683–1688.

(54) Weon, B. M.; Lee, J. S.; Je, J. H.; Fezzaa, K. X-ray-induced water vaporization. *Physical Review E* **2011**, *84*, 32601.

(55) Bras, W.; Stanley, H. Unexpected effects in non crystalline materials exposed to X-ray radiation. *Journal of Non-Crystalline Solids* **2016**, *451*, 153–160.

(56) Dupuy, R.; Bertin, M.; Féraud, G.; Romanzin, C.; Putaud, T.; Philippe, L.; Michaut, X.; Jeseck, P.; Cimino, R.; Baglin, V.; Fillion, J.-H. X-ray induced desorption and photochemistry in CO ice. *Physical Chemistry Chemical Physics* **2021**, *23*, 15965–15979.

(57) Chang, W. C.; Huang, L. C. L.; Wang, Y.-S.; Peng, W.-P.; Chang, H. C.; Hsu, N. Y.; Yang, W. B.; Chen, C. H. Matrix-assisted laser desorption/ionization (MALDI) mechanism revisited. *Analytica Chimica Acta* **2007**, *582*, 1–9.

(58) Navarro-González, R.; Negrón-Mendoza, A.; Chacón, E. The γ-irradiation of aqueous solutions of urea. Implications for chemical evolution. *Origins of life and evolution of the biosphere* **1989**, *19*, 109–118.

(59) Shakya, Y.; Inhester, L.; Arnold, C.; Welsch, R.; Santra, R. Ultrafast time-resolved x-ray absorption spectroscopy of ionized urea and its dimer through ab initio nonadiabatic dynamics. *Structural Dynamics* **2021**, *8*, 034102.

(60) Wang, F.; Ma, S.; Zhang, D.; Cooks, R. G. Proton Affinity and Gas-Phase Basicity of Urea. *The Journal of Physical Chemistry A* **1998**, *102*, 2988–2994.

(61) Minenkov, Y.; Wang, H.; Wang, Z.; Sarathy, S. M.; Cavallo, L. Heats of Formation of Medium-Sized Organic Compounds from Contemporary Electronic Structure Methods. *Journal of Chemical Theory and Computation* **2017**, *13*, 3537–3560.

(62) Iyer, S.; Lopez-Hilfiker, F.; Lee, B. H.; Thornton, J. A.; Kurtén, T. Modeling the Detection of Organic and Inorganic Compounds Using Iodide-Based Chemical Ionization. *The Journal of Physical Chemistry A* **2016**, *120*, 576–587.

(63) Finkenzeller, H. et al. The gas-phase formation mechanism of iodic acid as an atmospheric aerosol source. *Nature Chemistry* **2023**, *15*, 129–135.

(64) Hunter, E. P. L.; Lias, S. G. Evaluated Gas Phase Basicities and Proton Affinities of Molecules: An Update. *Journal of Physical and Chemical Reference Data* **1998**, *27*, 413–656.

(65) Kaftory, M.; Kapon, M.; Botoshansky, M. Role of Hydrogen Bonding in Determining the Crystal Structures of the Adducts between Acetone and Urea Derivatives. *Chemistry of Materials* **1994**, *6*, 1245–1249.

(66) Iyer, S.; He, X.; Hyttinen, N.; Kurtén, T.; Rissanen, M. P. Computational and Experimental Investigation of the Detection of HO2 Radical and the Products of Its Reaction with Cyclohexene Ozonolysis Derived RO2 Radicals by an Iodide-Based Chemical Ionization Mass Spectrometer. *The Journal of Physical Chemistry A* **2017**, *121*, 6778–6789.

(67) Shen, J. et al. High Gas-Phase Methanesulfonic Acid Production in the OH-Initiated Oxidation of Dimethyl Sulfide at Low Temperatures. *Environ. Sci. Technol.* **2022**,

(68) Berndt, T. Methanesulfonic acid (MSA) and SO3 formation from the addition channel of atmospheric dimethyl sulfide oxidation. *Chem. Commun.* **2025**, *61*, 1443–1446.

(69) Ge, X.; Wexler, A. S.; Clegg, S. L. Atmospheric amines – Part I. A review. *Atmospheric Environment* **2011**, *45*, 524–546.

(70) Kanawade, V. P.; Jokinen, T. Atmospheric amines are a crucial yet missing link in Earth's climate via airborne aerosol production. *Communications Earth & Environment* **2025**, *6*, 98.

(71) Sellegri, K.; Hanke, M.; Umann, B.; Arnold, F.; Kulmala, M. Measurements of organic gases during aerosol formation events in the boreal forest atmosphere during QUEST. *Atmospheric Chemistry and Physics* **2005**, *5*, 373–384.

(72) Hanson, D. R.; McMurry, P. H.; Jiang, J.; Tanner, D.; Huey, L. G. Ambient Pressure Proton Transfer Mass Spectrometry: Detection of Amines and Ammonia. *Environmental Science & Technology* **2011**, *45*, 8881–8888.

(73) Zheng, J.; Ma, Y.; Chen, M.; Zhang, Q.; Wang, L.; Khalizov, A. F.; Yao, L.; Wang, Z.; Wang, X.; Chen, L. Measurement of atmospheric amines and ammonia using the high resolution time-of-flight chemical ionization mass spectrometry. *Atmospheric Environment* **2015**, *102*, 249–259.

(74) Pfeifer, J.; Simon, M.; Heinritzi, M.; Piel, F.; Weitz, L.; Wang, D.; Granzin, M.; Müller, T.; Bräkling, S.; Kirkby, J.; Curtius, J.; Kürten, A. Measurement of ammonia, amines and iodine compounds using protonated water cluster chemical ionization mass spectrometry. *Atmospheric Measurement Techniques* **2020**, *13*, 2501–2522.

(75) Nowak, J. B.; Huey, L. G.; Eisele, F. L.; Tanner, D. J.; Mauldin III, R. L.; Cantrell, C.; Kosciuch, E.; Davis, D. D. Chemical ionization mass spectrometry technique for detection of dimethylsulfoxide and ammonia. *Journal of Geophysical Research: Atmospheres* **2002**, *107*, 10–1.

(76) Nowak, J. B.; Huey, L. G.; Russell, A. G.; Tian, D.; Neuman, J. A.; Orsini, D.; Sjostedt, S. J.; Sullivan, A. P.; Tanner, D. J.; Weber, R. J.; Nenes, A.; Edgerton, E.; Fehsenfeld, F. C. Analysis of urban gas phase ammonia measurements from the 2002 Atlanta Aerosol Nucleation and Real-Time Characterization Experiment (ANARChE). *Journal of Geophysical Research: Atmospheres* **2006**, *111*.

(77) Benson, D. R.; Markovich, A.; Al-Refai, M.; Lee, S.-H. A Chemical Ionization Mass Spectrometer for ambient measurements of Ammonia. *Atmospheric Measurement Techniques* **2010**, *3*, 1075–1087.

(78) Nowak, J. B.; Neuman, J. A.; Kozai, K.; Huey, L. G.; Tanner, D. J.; Holloway, J. S.; Ryerson, T. B.; Frost, G. J.; McKeen, S. A.; Fehsenfeld, F. C. A chemical ionization mass spectrometry technique for airborne measurements of ammonia. *Journal of Geophysical Research: Atmospheres* **2007**, *112*.

(79) Dong, F.; Li, H.; Liu, B.; Liu, R.; Hou, K. Protonated acetone ion chemical ionization time-of-flight mass spectrometry for real-time measurement of atmospheric ammonia. *Journal of Environmental Sciences* **2022**, *114*, 66–74.

(80) Yu, H.; Lee, S.-H. Chemical ionisation mass spectrometry for the measurement of atmospheric amines. *Environmental Chemistry* **2012**, *9*, 190–201.

(81) You, Y. et al. Atmospheric amines and ammonia measured with a chemical ionization mass spectrometer (CIMS). *Atmospheric Chemistry and Physics* **2014**, *14*, 12181–12194.

(82) Sipilä, M.; Sarnela, N.; Jokinen, T.; Junninen, H.; Hakala, J.; Rissanen, M. P.; Praplan, A.; Simon, M.; Kürten, A.; Bianchi, F.; Dommen, J.; Curtius, J.; Petäjä, T.; Worsnop, D. R. Bisulfate –

cluster based atmospheric pressure chemical ionization mass spectrometer for high-sensitivity (¡ 100 ppqV) detection of atmospheric dimethyl amine: proof-of-concept and first ambient data from boreal forest. *Atmospheric Measurement Techniques* **2015**, *8*, 4001–4011.

(83) Grönberg, L.; Lövkvist, P.; Jönsson, J. A. Determination of aliphatic amines in air by membrane enrichment directly coupled to a gas chromatograph. *Chromatographia* **1992**, *33*, 77–82.

(84) Huang, W.; Li, H.; Sarnela, N.; Heikkinen, L.; Tham, Y. J.; Mikkilä, J.; Thomas, S. J.; Donahue, N. M.; Kulmala, M.; Bianchi, F. Measurement report: Molecular composition and volatility of gaseous organic compounds in a boreal forest – from volatile organic compounds to highly oxygenated organic molecules. *Atmospheric Chemistry and Physics* **2021**, *21*, 8961–8977.

(85) Brandner, J. D.; Junk, N. M.; Lawrence, J. W.; Robins, J. Vapor Pressure of Ammonium Nitrate. *Journal of Chemical & Engineering Data* **1962**, *7*, 227–228.

(86) Chien, W.-M.; Chandra, D.; Lau, K. H.; Hildenbrand, D. L.; Helmy, A. M. The vaporization of NH4NO3. *The Journal of Chemical Thermodynamics* **2010**, *42*, 846–851.

Graphical Abstract to:
Uronium from X-ray Desorbed Solid Urea Enables Attomole Sensitivity to Amines and Semivolatiles

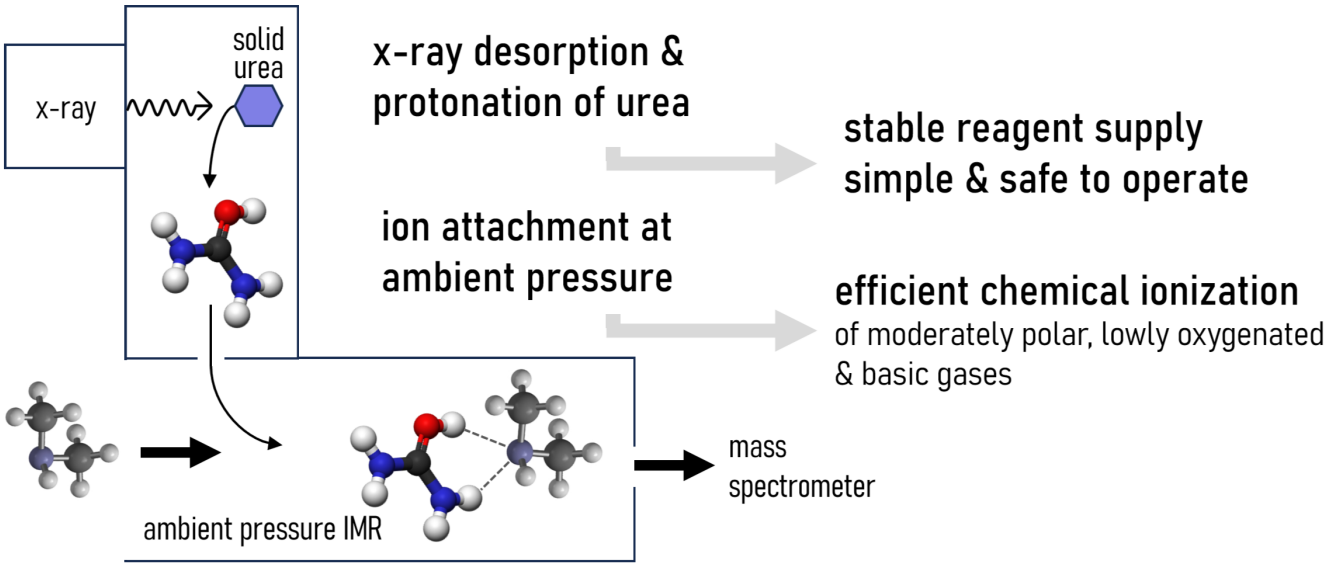

Supplementary Information to:
Uronium from X-ray Desorbed Solid Urea Enables Attomole Sensitivity to Amines and Semivolatiles

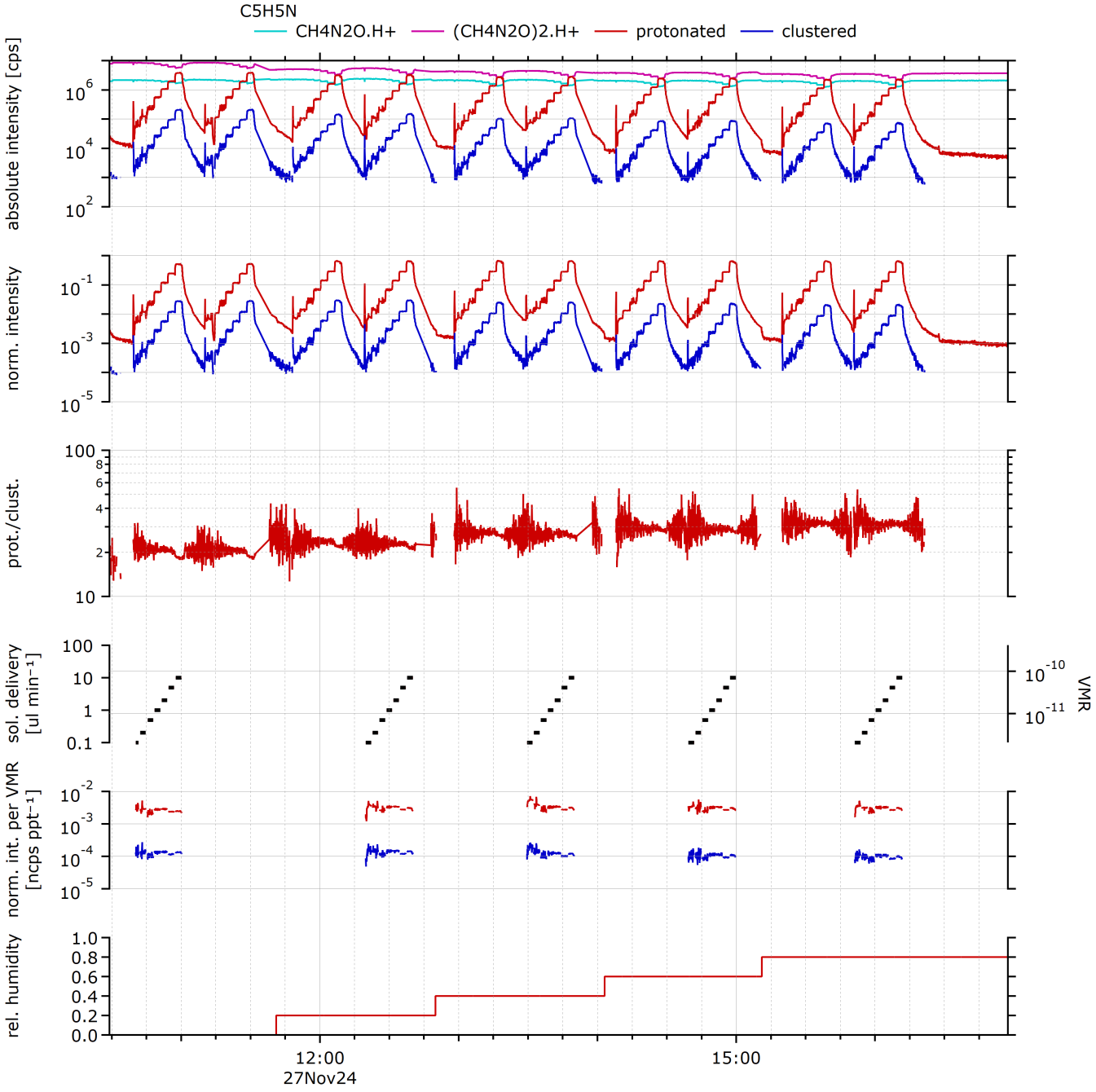

Figure S1: Calibration experiment example (pyridine, C_5H_5N): Time series of the raw intensities, normalized intensity, ratio of protonated and cluster signal, delivery rate for solution to liquid calibration unit, ratio of normalized intensity to volume mixing ratio, and relative humidity.

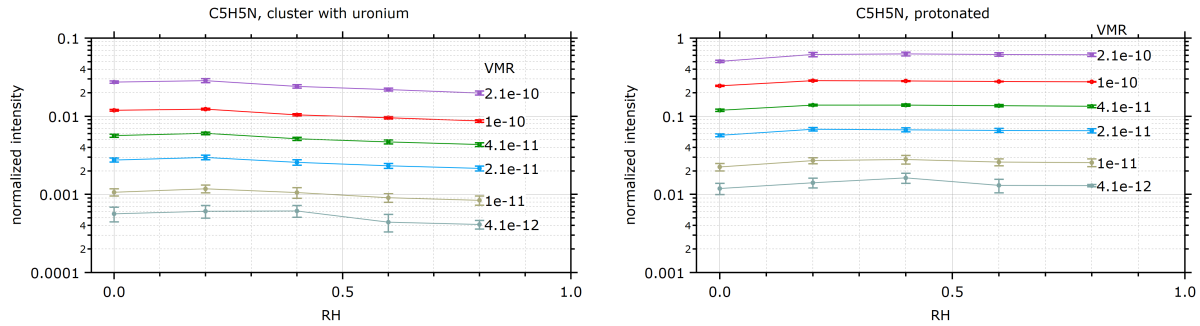

Figure S2: Calibration experiment example (pyridine, C_5H_5N): Normalized intensity as function of relative humidity, for different dosing ratios.

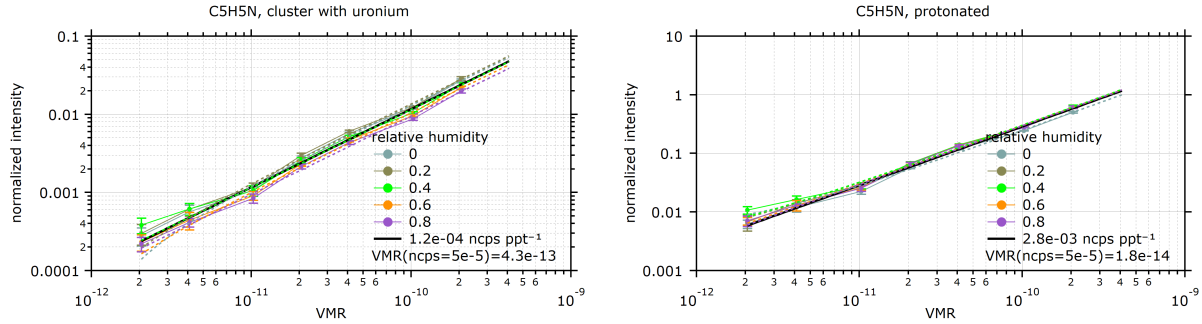

Figure S3: Calibration experiment example (pyridine, C_5H_5N): Normalized intensity as function of dosed volume mixing ratio, for different humidities.

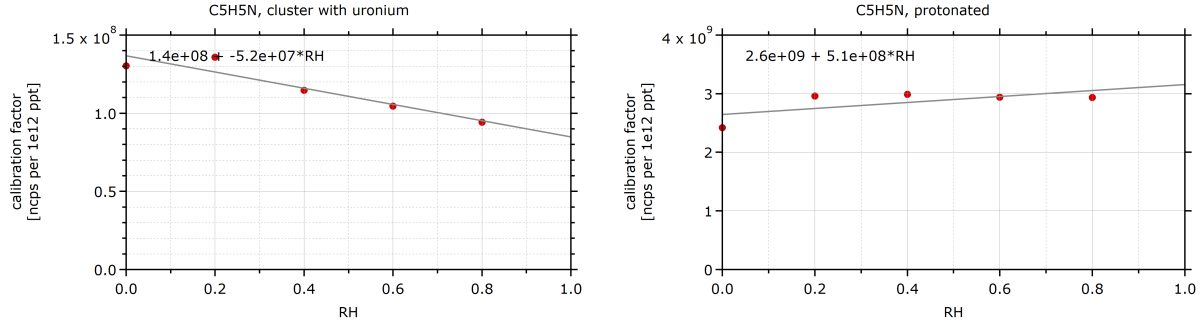

Figure S4: Calibration experiment example (pyridine, C_5H_5N): Calibration factor as function of relative humidity.

Table S1: Calculated enthalpies for fragmentation of the target–uronium cluster into analyte (M) and uronium (UH^+)), and protonated analyte (MH^+) and urea (U).

target	sum formula	$MUH^+ \rightarrow M + UH^+$ kcal mol^{-1}	$MUH^+ \rightarrow MH^+ + U$ kcal mol^{-1}
acetaldehyde	C_2H_4O	25.32	50.44
catechol	$C_6H_6O_2$	24.52	52.20
dimethylformamide	C_3H_7NO	34.91	35.24
dimethyl sulfoxide	C_2H_6OS	36.63	33.51
furfural	$C_5H_4O_2$	29.75	37.11
guaiacol	$C_7H_8O_2$	24.14	48.65
pinonealdehyde	$C_{10}H_{16}O$	35.36	28.97
pyridine	C_5H_5N	38.76	25.44
syringol	$C_8H_{10}O_3$	32.40	49.63
verbenone	$C_{10}H_{14}O$	36.11	30.70
urea	CH_4N_2O	35.16	35.16
ammonia	NH_3	26.88	32.51
benzylamine	C_7H_9N	39.44	27.89
diethylamine	$C_4H_{11}N$	43.53	25.31
diisopropylamine	$C_6H_{15}N$	23.70	1.44
dimethylamine	C_2H_6NH	40.05	27.15
water	H_2O	20.56	64.91
methanol	CH_3OH	23.57	52.48
methylamine	CH_3NH_2	35.38	29.84
phenylethylamine	$C_8H_{11}N$	40.11	26.22
trimethylamine	C_3H_9N	43.03	25.51
acetone	C_3H_6O	28.04	43.06
ethylamine	C_2H_6NH	36.79	28.08
PGMEA[a]	$C_6H_{12}O_3$	35.42	29.83
trimethylsilanol	$C_3H_{10}OSi$	25.56	41.59
hexamethyldisiloxane	$C_6H_{19}NSi_2$	37.23	21.25
glyoxal	$C_2H_2O_2$	20.01	64.47
methylpyrrolidone	C_5H_9NO	37.65	28.56
dimethyl selenoxide	C_2H_6OSe	43.03	82.02
iodine	I_2	10.32	
iodine oxide	IO	22.52	
iodine dioxide	OIO	21.59	
diiodine dioxide	I_2O_2	33.47	
diiodine trioxide	I_2O_3	29.54	
diiodine tetroxide	I_2O_4	35.51	
diiodine pentoxide	$IOIO_4$	25.90	
hypoiodous oxide	HOI	19.54	
iodous oxide	HIO_2	33.80	
iodic oxide	HIO_3	27.44	

a: propylene glycol methyl ether acetate

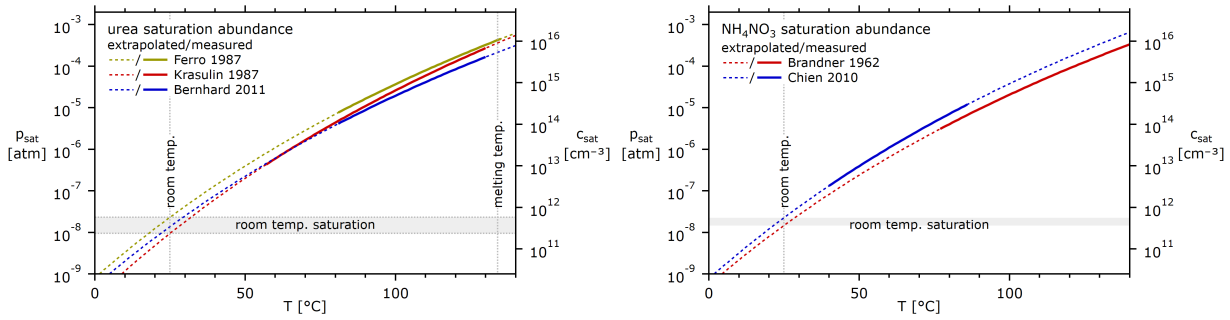

Figure S5: Saturation abundance of urea and ammonium nitrate in measurements and extrapolated to room temperature.

Ferro, D., Barone, G., della Gatta, G. & Piacente, V. Vapour pressures and sublimation enthalpies of urea and some of its derivatives. The Journal of Chemical Thermodynamics 19, 915–923 (1987).

Krasulin, A. P., Kozyro, A. A. & Kabo, G. Ya. Saturation vapor pressure of urea in the temperature range 329-403 K. 60, 96–99 (1987).

Bernhard, A. M., Czekaj, I., Elsener, M., Wokaun, A. & Kröcher, O. Evaporation of Urea at Atmospheric Pressure. The Journal of Physical Chemistry A 115, 2581–2589 (2011).

Brandner, J. D., Junk, N. M., Lawrence, J. W. & Robins, J. Vapor Pressure of Ammonium Nitrate. Journal of Chemical & Engineering Data 7, 227–228 (1962).

Chien, W.-M., Chandra, D., Lau, K. H., Hildenbrand, D. L. & Helmy, A. M. The vaporization of NH4NO3. The Journal of Chemical Thermodynamics 42, 846–851 (2010).

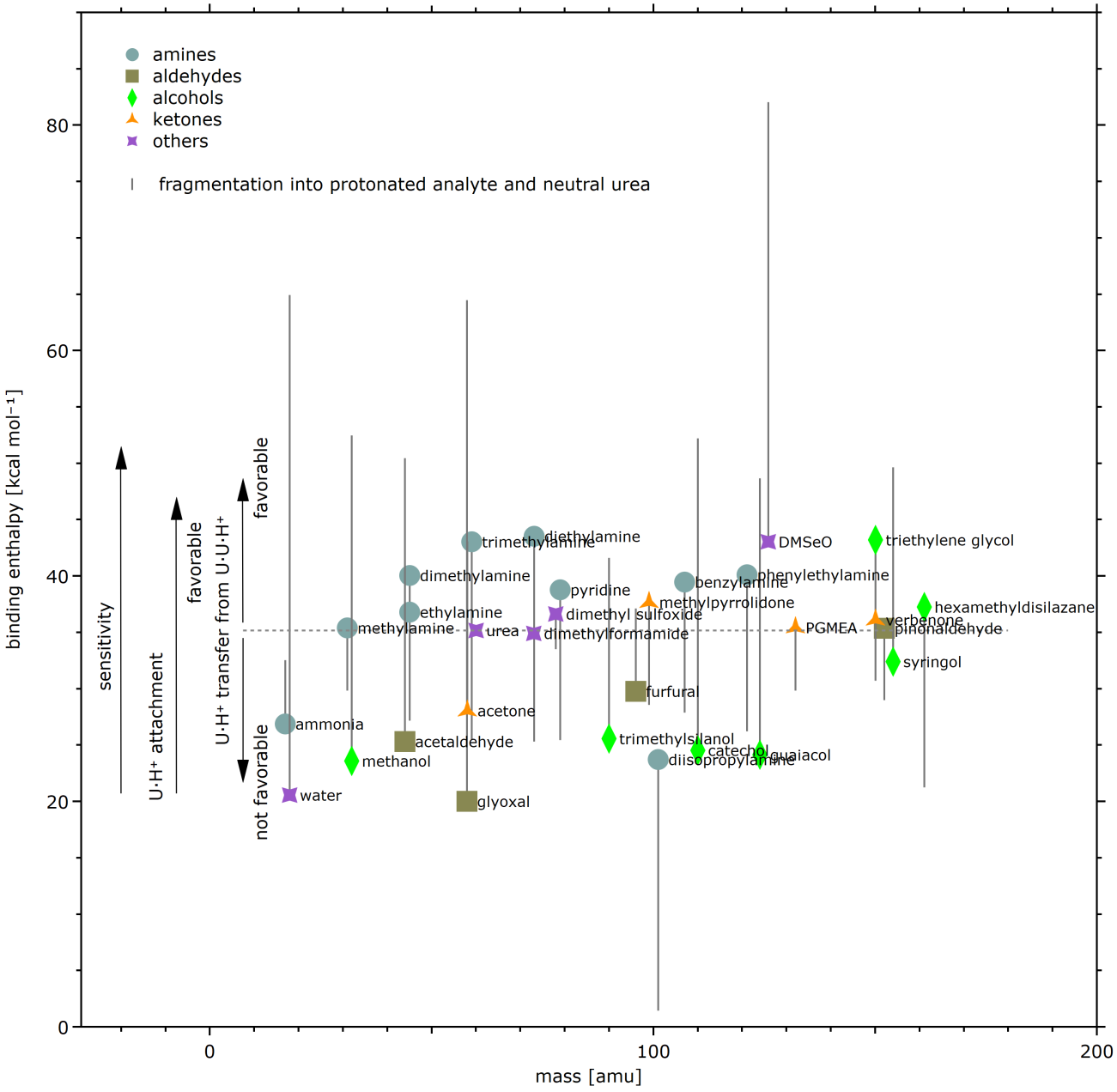

Figure S6: Calculated binding enthalpies for the formation of analyte–uronium clusters for compounds of different classes. Same as in main text Fig. 4, but including also the enthalpy of fragmentation of the analyte–uronium cluster into protonated analyte and neutral urea (end of thin lines). The abbreviations refer to the following compounds: U: urea; PGMEA: propylene glycol methyl ether acetate; DMSeO: dimethyl selenoxide.

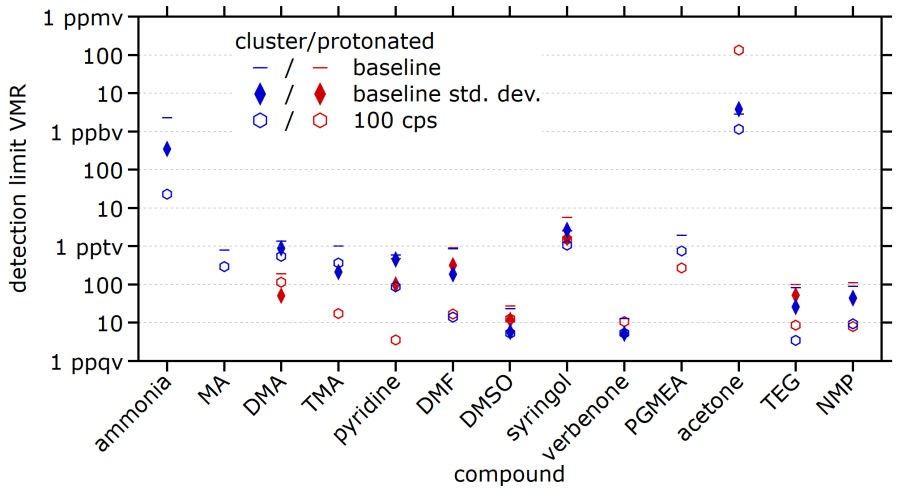

Figure S7: Detection limits for different compounds either as cluster with uronium (blue markers) or protonated (red markers). The detection limits are estimated in different ways: First, the horizontal lines indicate is the volume mixing ratio equivalent to the instrument background (if present) when the inlet is overflowed with pure nitrogen. The diamond marker indicate the detection limit calculated as three times the standard deviation of a the instrument background (if present). Lastly, the hexagonal marker is the volume mixing ratio equivalent to 100 cps signal, the approximately lowest signals still detectable.